Precipitation and nonlinear effects in geomagnetic field line resonances

M. Prakash[1] and R. Rankin
Department of Physics, University of Alberta, Edmonton, Alberta, Canada

V. T. Tikhonchuk
Institut de Physique Fondamentale, Univesité Bordeaux 1, France

Received 14 March 2002; revised 5 July 2002; accepted 15 July 2002; published 26 March 2003.

[1] The structure of auroral arcs sustained by field line resonances (FLRs) is determined using a model that describes the interplay between ionospheric feedback, nonlinear, and dispersive effects in a curvilinear geomagnetic topology. The model includes modulation of Pedersen conductance by hundreds of eV electrons that precipitate in the ionosphere through the action of shear Alfvén wave field-aligned currents (FACs). The competition between ionospheric feedback dissipation, wave dispersion, and nonlinearity results in large-amplitude, long-period oscillations of the FAC, and in emission of slow-moving small-scale secondary auroral arcs and density perturbations. Using observed values of nightside conductivities and realistic topology of geomagnetic field lines, we obtain FLRs with frequencies in the range of a few mHz, spatial scales up to several km near the ionosphere, and FAC amplitudes extending to tens of $\mu A/m^2$. Our model explains the excitation of structured auroral arcs in regions of low ionospheric conductance. *INDEX TERMS:* 2407 Ionosphere: Auroral ionosphere (2704); 2704 Magnetospheric Physics: Auroral phenomena (2407); 2716 Magnetospheric Physics: Energetic particles, precipitating; 2736 Magnetospheric Physics: Magnetosphere/ionosphere interactions

Citation: Prakash, M., R. Rankin, and V. T. Tikhonchuk, Precipitation and nonlinear effects in geomagnetic field line resonances, *J. Geophys. Res.*, *108*(A4), 8014, doi:10.1029/2002JA009383, 2003.

1. Introduction

[2] The formation of latitudinally narrow auroral arcs, and their connection with much larger-scale global magnetospheric processes, remains an outstanding problem in auroral physics. Discrete auroral arcs have been measured for more than 40 years by *Akasofu* [1961], *Maggs and Davis* [1968], *Borovsky et al.* [1991], *Knudsen et al.* [2001], *Trondsen and Cogger* [1998], and others. Many theories have been developed to explain different aspects of auroral arcs. However, as reported by *Borovsky* [1993], none of the existing theories is completely satisfactory. It is therefore important to develop new models that advance our understanding of physical processes that play a key role in the formation and structuring of auroral arcs [*Prakash and Lysak*, 1992; *Knudsen*, 1996; *Streltsov and Lotko*, 1997; *Streltsov et al.*, 1998; *Rankin et al.*, 1999a].

[3] The motivation for this paper is provided by ground-based observations [*Xu et al.*, 1993; *Samson et al.*, 1991, 1996], and more recent satellite observations [*Lotko et al.*, 1998], where a field line resonance (FLR) structure was observed simultaneously by the FAST satellite and instruments of the CANOPUS array. The FAST/CANOPUS observations of a discrete auroral arc have been attributed to a class of ultra low frequency FLRs (frequencies in the range of a few mHz) [*Hughes*, 1994] that accumulate energy $\sim 10^8$ J in the nightside magnetosphere between 6 and 15 Earth radii [*Greenwald and Walker*, 1980]. We present results from a new model of FLRs that incorporates ionospheric feedback, nonlinear, and dispersive effects in a curvilinear magnetic topology. Our model describes the properties of auroral arcs with spatial scales of several km that are temporally modulated at frequencies of a few mHz [*Samson et al.*, 1991].

[4] Ionospheric conductance plays an important role in the formation and structuring of auroral arcs. In particular, *Newell et al.* [1996] examined nine years of electron precipitation data from the DMSP spacecraft, and reported that intense (greater than 5 mW/m^2) discrete auroral arcs, associated with large-scale optical aurora [*Kletzing et al.*, 1983], are suppressed by sunlight, and are more likely to occur during darkness (winter) than sunlight (summer). The authors attribute this finding to an *ionospheric feedback instability* [*Atkinson*, 1970; *Holzer and Sato*, 1973; *Lysak*, 1986, 1990, 1991; *Lyatsky and Hamza*, 2000] that corresponds to a modulation of currents (driven by magnetospheric convection) by precipitating electrons. In this process, the field-aligned current (FAC) becomes unstable,

[1]Also at Department of Physics and Astronomy, SUNY at Stony, Stony Brook, New York, USA.

0148-0227/03/2002JA009383

causing growth of a drifting density perturbation in the ionosphere. This results in a periodic enhancement of the Pedersen conductance, and in the generation of shear Alfvén waves (SAWs) propagating into the magnetosphere. The feedback instability is effective at a low background conductance (around 1 mho), and is associated with SAWs with frequencies that are typically in the range 0.1–1 Hz. The instability domain is limited to frequencies determined by the electron recombination time in the ionosphere, which is approximately 100 s [*Rees*, 1963; *Lysak*, 1991].

[5] The ionospheric feedback instability cannot be applied to FLRs in the mHz frequency range because their periods are much longer than the electron recombination time. Here, we investigate a different mechanism of ionospheric feedback that is initiated by SAWs excited in FLRs. In this model, which does not involve magnetospheric convection, the FAC (associated with a SAW) changes the ionospheric Pedersen conductance by modulating the flux of precipitating electrons at the FLR frequency. The precipitating electrons increase the plasma density and decrease the SAW damping locally. The decrease in damping enhances the FAC, and thereby further reduces damping. Thus, a feedback loop is established, although it does not involve an instability.

[6] To accommodate ionospheric feedback into the FLR problem, we use the nonlinear dispersive field line resonance (NDFLR) model developed by *Frycz et al.* [1998] and *Rankin et al.* [1999a, 1999b], and modify it to account for nonlinear modulation of the ionospheric conductance. It will be shown that enhancement of ionospheric conductance in FLRs results in a stronger manifestation of dispersive and nonlinear effects such as wave structuring and excitation of density cavities by the SAW ponderomotive force. This is potentially quite important, as both theory and observations [*Persoon et al.*, 1988; *Génot et al.*, 2000] have demonstrated that density cavities are an essential ingredient of auroral arc physics.

[7] The paper is organized as follows: In section 2, we briefly discuss the important features of the NDFLR wave model in a curvilinear geomagnetic field. In section 3, we incorporate in the NDFLR model the modification of ionospheric conductance by precipitating electrons. The numerical results are presented in section 4 for a dipolar and stretched geomagnetic topology. We analyze the effects of dispersion, dissipation, and nonlinearities in the enhancement and structuring of the FAC. Section 5 summarizes our results.

2. Nonlinear Dispersive FLR Model

[8] We begin by summarizing the model of nonlinear dispersive field line resonances (NDFLR) discussed by [*Frycz et al.*, 1998; *Rankin et al.*, 1999a, 1999b]. The model describes resonant excitation of SAWs by a monochromatic driver, which represents a global compressional Alfvén wave in the magnetospheric cavity [*Kivelson and Southwood*, 1986]. This resonant SAW is a toroidal eigenmode standing between the Northern and Southern parts of the Earth's ionosphere [*Taylor and Walker*, 1984] and may propagate across magnetic surfaces due to dispersion effects [*Hasegawa*, 1976; *Goertz*, 1984]. The model also accounts for SAW damping due to Joule heating of the ionosphere by the Pedersen current, and includes nonlinear detuning of the resonance by the ponderomotive force. The model is based on the equation for the SAW amplitude coupled with the equation for the ion density perturbations that are driven by the SAW ponderomotive force.

[9] The SAW equation is derived by casting the reduced magneto-hydrodynamic (MHD) equations into a curvilinear geometry [*Rankin et al.*, 1999a, 1999b]. The azimuthal component of the SAW magnetic field is presented in the envelope approximation, $h_\phi B_\phi = h_\phi^{eq} B_0^{eq}$ Reb (x, t) $S_0(l)$ exp $i(m\phi - \omega_0 t)$, and the dimensionless amplitude b satisfies the following equation:

$$\partial_t b - (i/2)\omega\delta\partial_x^2 b = i(\delta\Omega - \Delta\omega)b + \frac{\omega_0}{2}R. \tag{1}$$

[10] Here, S_0 is the fundamental toroidal eigenmode (without accounting for damping and dispersion effects) that forms the FLR along the geomagnetic field line, and ω_0 is the frequency of the external compressional driver.

[11] The wave field in equation (1) is defined in a curvilinear coordinate system, where μ is the coordinate along the magnetic field line, ν is the flux coordinate, ϕ is the azimuthal angle, (h_μ, h_ν, h_ϕ) are the corresponding metric coefficients, and m is the azimuthal mode number (we consider low-m modes only). The field aligned coordinate is defined as $dl = h_\mu d\mu$ (with the origin located at $l = 0$ in the equatorial plane), B_0^{eq} is the equatorial magnetic field ($B_0(l) = B_0^{eq} h_\mu^{eq}/h_\mu(l)$), and the perpendicular (radial in the equatorial plane) coordinate is defined as $dx = h_\nu^{eq} d_\nu$ with the origin ($x = 0$) lying on the resonant geomagnetic field line where the driver frequency is equal to the eigenfrequency of the toroidal eigenmode.

[12] The quantity $\Delta\omega = \omega_0 x/2l_\omega - i\gamma$ in equation (1) is the complex frequency detuning. Its real part accounts for the variation of the FLR eigenfrequency across magnetic surfaces. The perpendicular length scale l_ω is related to the characteristic spatial scale of the Alfvén speed profile around the resonant line in the equatorial plane. The imaginary part accounts for dissipation due to the coupling of the FAC with the ionospheric Pedersen current [*Rankin et al.*, 1999a]

$$\gamma = \frac{1}{\mu_0 \Sigma_p N}\left[S_0^2 h_\nu/h_\phi\right]_{l_{max}}. \tag{2}$$

Here, Σ_p is the ionospheric Pedersen conductance, the numerator is evaluated at the ionospheric end of the magnetic field line at $l = l_{max}$, and $N = 2\int_0^{l_{max}} dl\, S_0^2 h_\nu/h_\phi$ is a normalization factor. Near the ionosphere, the damping is associated with a quadrature component of the radial electric field in the ionosphere that satisfies the boundary condition $\mu_0 \Sigma_p E_x = \pm B_\phi$ at $l = \pm l_{max}$ [*Taylor and Walker*, 1984; *Lysak*, 1990].

[13] The quantity R in equation (1) represents the effect of the compressional driver with an amplitude B_c that excites the FLR,

$$R = -\frac{1}{2N\omega_0^2 h_\phi^{eq} B_0^{eq}} \int dl \frac{h_\nu}{h_\phi} V_A^2 B_c \frac{\partial S_0}{\partial l} \tag{3}$$

where V_A is the local Alfvén speed. The SAW dispersion parameter δ stands for the local dispersion averaged along the resonant field line:

$$\delta = \frac{\left(h_\nu^{eq}\right)^2}{N} \int \frac{dl}{h_\mu} \left[\frac{3}{4} \frac{\rho_i^2 V_A^2}{\omega_0^2} \left(\frac{\partial S_0}{\partial l} \right)^2 + \frac{V_{Te}^2}{\omega_0^2} \frac{\partial S_0}{\partial l} \frac{\partial S_0 \lambda_e^2}{\partial l} - \lambda_e^2 S_0^2 \right]. \tag{4}$$

[14] Here, ρ_i is the ion-gyroradius, λ_e is the electron inertial length, and V_{Te} is the electron thermal speed. These parameters correspond to three physical effects which contribute to SAW dispersion. Electron thermal effects (the second term in equation (4)) dominate FLR dynamics if the characteristic electron bounce period, $l_{max}/V_{Te} \sim 60$ s, is shorter than the wave period. The effects of wave dispersion are rather complicated in this regime due to the non-local response of electrons to the FAC carried by SAWs [*Rankin et al.*, 1999c]. This is particularly important for determining parallel electric fields in FLRs. The structure and nonlinear evolution of parallel electric fields is outside the scope of the present analysis. However, at low frequencies, we use values of δ calculated from the kinetic theory because they are crucial to obtaining proper perpendicular scales of the FLR wave fields at saturation.

[15] Equation (1) also contains the nonlinear frequency detuning parameter $\delta\,\Omega = \Sigma_M n_M g_M$ that arises from density perturbations driven by the ponderomotive force of SAWs [*Rankin et al.*, 1995]:

$$\delta\Omega = \frac{1}{2\omega_0 N} \int dl V_A^2 \frac{h_\nu}{h_\phi} \frac{\delta\rho}{\rho_0} \left(\frac{\partial S_0}{\partial l} \right)^2. \tag{5}$$

[16] The changes in the ambient plasma density lead to a corresponding change in the local Alfvén velocity and in the eigenfrequency of the FLR. This results in a frequency mismatch with the driver and causes a saturation of the SAW amplitude. The pressure perturbation δP and the density perturbation $\delta\rho = \delta P/C_s^2$ are represented as a sum over the ion acoustic wave eigenfunctions: $\delta P = P_0^{eq} \Sigma_M n_M (x, t)\, U_M(l)$. The eigenfunctions $U_M(l)$, and the eigenfrequencies Ω_M, are solutions of the linearized density equation. They are pre-calculated (typically 7–10 modes are used) for a given topology of the magnetic field lines.

[17] The time evolution of density perturbations is described by the ion acoustic wave equation,

$$\partial_t^2 n_M + 2\Gamma_I \partial_t n_m + \Omega_M^2 n_m = \frac{\omega_0^2}{2} f_M \mid b \mid^2 \tag{6}$$

where Γ_I is the damping coefficient of mode M, C_s is the ion acoustic speed, and the coupling coefficients f_M and g_M represent the projection of the SAW ponderomotive force on the M-th ion acoustic wave mode, and the contribution of the mode to the frequency detuning, respectively.

[18] Equations (1) and (6) describe the nonlinear evolution of amplitudes of the azimuthal component of the FLR magnetic field and ion acoustic density perturbations. In particular, the dispersive and damping terms in the SAW equation define the FLR width. By comparing the dispersion and detuning terms in equation (1) one finds the characteristic dispersion width at the equatorial plane

$$\Delta x_{disp} \approx (l_\omega \delta)^{1/3}. \tag{7}$$

Correspondingly, the comparison between the dissipation and detuning terms defines the dissipation width

$$\Delta x_{diss} \approx l_\omega \gamma/\omega_0. \tag{8}$$

The analysis of solutions to equation (1) by *Frycz et al.* [1998] demonstrates that among these two processes, the dominant one is that which yields the larger width: $\Delta x_0 = \max\{\Delta x_{disp}, \Delta x_{diss}\}$. The FLR width at the distance l from the equatorial plane $\Delta x(l) = \Delta x_0/h_x(l)$ can be calculated by using the radial scaling factor $h_x(l) = h_\nu^{eq}/h_\nu(l)$.

3. NDFLR Model With FAC-Dependent Ionospheric Conductance

[19] The Pedersen conductance is one of the important parameters in the NDFLR model. It is provided by free electrons that are created in the ionosphere by cosmic and solar radiation and, subsequently, transported by currents flowing across magnetic field lines. Electrons that precipitate in the ionosphere by the action of SAW wave fields also produce additional ionization. This can change the SAW dissipation and has an important effect on FLR dynamics. We describe here how precipitation-induced changes in the ionospheric ionization can be incorporated into the NDFLR model. Our derivation corrects errors in the preliminary studies of *Prakash and Rankin* [2001], whose derivation is inconsistent with the envelope ansatz for the SAW dynamics. Since the characteristic electron-ion recombination time of about 100 s in the ionosphere [*Lysak*, 1991], is shorter than the SAW period, we use the quasi-static approximation. Then, the ionospheric plasma density is defined by the balance equation, $S_e + S_c = \alpha\, n_e^2$, where α is the recombination rate, S_c is the ionization source due to cosmic radiation, and S_e is the ionization produced by precipitating electrons. Since the Pedersen conductance is proportional to the electron density, $\Sigma_p \propto n_e$, and the ionization rate is proportional to the energy flux, ϵ, of precipitating electrons, $S_e \propto \epsilon$, one arrives at the following root-mean-square relation for the Pedersen conductance [*Reiff*, 1984]

$$\Sigma_p = \left(\Sigma_0^2 + Q^2 \epsilon\right)^{1/2} \tag{9}$$

where Σ_0 is the background Pedersen conductance and Q is an empirical coefficient. This expression is more accurate than the arithmetic sum of the conductivities empirically proposed by *Lyons* [1980].

[20] By fitting the quantity $Q\epsilon^{1/2}$ with electron precipitation data from spacecraft, it was suggested $Q = 160$ mho m/W$^{1/2}$ [*Lyons*, 1980; *Harel et al.*, 1981]. Later *Spiro et al.* [1982] accounted for the dependence of the ionization rate on the energy K_e of precipitating electrons. For K_e expressed in keV, and Q expressed in mho–m/W$^{1/2}$, it was suggested that $Q = 630\, K_e/(4 + K_e^2)$. *Robinson et al.* [1987] pointed out that this result is based on an incorrect assumption that the characteristic energy of the electron

distribution function is equal to the average energy, while for a Maxwellian distribution the average energy is twice its characteristic energy. Robinson's formula with the appropriate correction yields: $Q = 1260\ K_e/(16 + K_e^2)$. From this expression, it is evident that Q increases with energy, peaks, and then decreases. At the peak value, $K_e = 4$ keV, the Pedersen conductance in Robinson's model attains the same value as given by Lyons's relation, provided the energy fluxes are identical.

[21] The energy flux of precipitating electrons, $\epsilon = K_e n_e v\mu$, depends on the electron kinetic energy and velocity v_μ parallel to the geomagnetic field line. It is related to the SAW field-aligned electric current, $J_\mu = -en_e v_\mu$, as follows: $\epsilon = -J_\mu K_e/e$, if $J_\mu < 0$, and $\epsilon = 0$ if $J_\mu > 0$. The latter relation accounts for the fact that there is no precipitation in the downward current region and the ionospheric conductance increases over the ambient value only in periods of negative (upward) FAC. In this formalism, we neglect the mirror force effect on the electrons. This is justified because, the NDFLR model calculates the FAC at the foot of the magnetic field line, just above the ionosphere. The input to the conductance model is the electron energy flux and the electron energy. We have considered the electron temperature as a measure of the average electron energy. No mirror force is required at this level, because the inhomogeneity of the parallel magnetic field does not play a significant role within the dissipation layer of the ionosphere.

[22] According to *Rankin et al.* [1999a], the relation between the FAC amplitude at the ionospheric level and the SAW amplitude reads:

$$\mu_0 J_\mu = B_0(l_{max}) S_0(l_{max}) \mathrm{Re}\, \partial_x b \exp(im\phi - i\omega_0 t). \qquad (10)$$

Combining equations (9) and (10), we obtain an expression for the Pedersen conductance in the presence of electron precipitation,

$$\Sigma_p = \Sigma_0 \left(1 + \sigma_p^2 \max\{0, \mathrm{Re}\partial_x b \exp(im\phi - i\omega_0 t)\}\right)^{1/2} \qquad (11)$$

where $\sigma_p = Q\ \Sigma_0^{-1}\ [K_e B_0(l_{max})\ S_0\ (l_{max})/e\ \mu_0]^{1/2}$. When this formula is substituted into equation (2), it describes SAW damping oscillating within the wave period. To be consistent with the envelope approximation, the quantity that enters in equation (1) is the damping averaged over the wave period $T = 2\pi/\omega_0$,

$$\bar{\gamma} = \frac{1}{T}\int_0^T dt\gamma(t) = \frac{\gamma_0}{T}\int_0^T dt \frac{\sum_0}{\sum_p(t)} \qquad (12)$$

where γ_0 is the SAW damping defined by equation (2), with the ambient conductance, Σ_0. Since electron precipitation changes the ionospheric conductance only during one half of the SAW period, we can represent the latter equation as follows

$$\bar{\gamma} = \frac{\gamma_0}{2}\left[1 + \frac{1}{\pi}\int_0^\pi \frac{d\alpha}{\left(1 + \sigma_p^2 \mid \partial_x b \mid \sin\alpha\right)^{1/2}}\right]. \qquad (13)$$

[23] Here, the second term accounts for the modification of SAW damping by electrons that impinge on the ionosphere during the half-cycle when the SAW current is upward. The integral in equation (13) has been evaluated numerically using a Gauss-Legendre quadrature formula. It can also be expressed in terms of elliptic functions. As a result of this expression, electron precipitation cannot reduce SAW damping by more than two times. Equation (13) is different from the one used by *Prakash and Rankin* [2001].

4. Numerical Results and Discussion

[24] In order to study the effect of modulation of ionospheric conductance on the formation and structure of an auroral arc, we solve the coupled equations (1) and (6) in the presence of electron precipitation-induced damping. We have used Robinson's model in equation (13) because it has a solid theoretical background and agrees with observations. We first consider the case of a dipolar magnetic field line mapping to a polar latitude of 67.5° (the dipolar index $L = 6.83$) which corresponds to the FLR event observed by the FAST satellite [*Lotko et al.*, 1998]. Next, we perform similar calculations in a stretched topology that provides a field-line eigenfrequency in the frequency range of observed nightside FLRs.

4.1. FLRs in the Dipolar Geometry

[25] Following *Streltsov and Lotko* [1997] and *Rankin et al.* [1999b], we define the density and ion temperature profiles along the magnetic field line: $\rho_0(\theta) = \rho_0^{eq} p(\theta)$ and $T_i(\theta) = T_i^{eq}/p(\theta)$, where $\rho_0^{eq} = 3.3$ amu and $T_i^{eq} = 1$ keV are the plasma density and the ion temperature in the equatorial plane. The function $p(\theta) = 0.77 + 0.23\cos^{-6}\theta + 1.7 \cdot 10^5 \exp[-(L\cos^2\theta - 1.05)/0.08]$ accounts for dependence on magnetic latitude θ and $L\cos^2\theta$ is geocentric distance to the magnetic field line expressed in units of the Earth radius, R_E. Then, for the dipolar line $L = 6.83$, one finds the SAW period is 66 s, corresponding to the frequency $\omega_0 = 15$ mHz, and the frequency detuning length $l_\omega = 0.7\ R_E$. For the typical values of Pedersen conductance on the nightside ionosphere, $\Sigma_0 = 0.8$ mho [*Lysak*, 1990], the SAW damping coefficient $\gamma_0/\omega_0 = 0.044$ corresponds to the SAW damping time of 240 s.

[26] In order to examine the role of dispersion and dissipation in the enhancement of FACs by the ionospheric feedback effect, we choose the value of the SAW dispersion $\delta = 1.25 \cdot 10^{-5} R_E^2$ such that the dispersive and dissipative FLR widths as given in equations (7) and (8) are of the same order. It will be shown later that this is the most favorable condition for nonlinear feedback. The positive sign of δ corresponds to the FLR case where electron thermal effects dominate [*Rankin et al.*, 1999a]. The driver amplitude $R = 7.3 \cdot 10^{-3}$ is chosen such that the amplitude of the wave magnetic field saturates (at the ionospheric level) around 150 nT, this value is consistent with observations by the FAST satellite [*Lotko et al.*, 1998].

[27] Figure 1 shows the time-dependence of the maximum amplitude of the FAC (at 4000 km altitude of the FAST orbit) across the resonance for the case where the driver is continuously on (top panel) and turned off after 5 SAW periods (bottom panel). The four curves in each panel

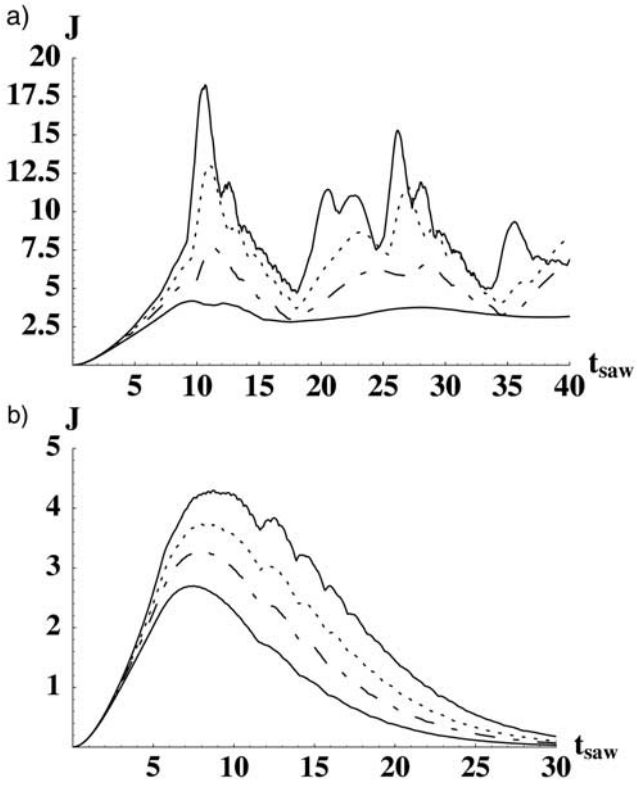

Figure 1. The field-aligned current (in $\mu A/m^2$) in FLRs as a function of time t normalized by the FLR wave period in a dipolar geometry. The solid curves correspond to a precipitation source of energy 350 eV (top curve) and to the case without precipitation (lower curve). The dotted and dash-dotted curves correspond to precipitation energies of 250 eV and 150 eV, respectively. The top panel refers to the continuous driver, while the bottom panel corresponds to the case when the driver is switched off after 5 SAW periods. The ambient Pedersen conductance $\Sigma_0 = 0.8$ mho, other parameters are explained in the text.

correspond to cases without precipitation, and with precipitation characterized by electron energies of 150 eV, 250 eV, and 350 eV, respectively. It can be seen in the upper panel that the FAC increases with an increase in energy of precipitating electrons and exhibits long-period nonlinear pulsations.

[28] The finite duration driver in Figure 1 illustrates the unforced FLR dynamics. In this case, the current continues to grow after the driver is turned off (during 2–3 SAW periods), and then it starts to decay. The period of growth without the driver is due to the finite dispersion in the system, and is affected by the electron precipitation energy. For example, the decay time with 350 eV electron precipitation is almost two times larger than the case without precipitation. This agrees with the qualitative estimate that follows from the nonlinear term in equation (13). It is found that the period of nonlinear pulsations for the case with a continuous driver is comparable to the decay time for the case where the driver is switched off after 5 periods.

[29] Figure 2 shows the dependence of FAC dynamics on the ambient conductance for cases without precipitation (upper panel) and with precipitation of 250 eV electrons (bottom panel). Comparing the top and bottom panels we note that for the chosen driver amplitude and precipitation energy, feedback is ineffective for conductances smaller than 0.8 mho. The temporal behavior is very similar in both cases although the FAC amplitude increases with the precipitation energy. At $\Sigma_p = 0.8$ mho, the dissipative width, $\Delta x_{diss} = 0.03\ R_E$ is larger than the dispersive width, $\Delta x_{disp} = 0.02\ R_E$. Therefore, for smaller conductances the dispersion effects are negligible and FLR dynamics is dissipative. At conductances higher than 0.8 mho, the electron precipitation increases the FAC more significantly and produces large-scale oscillations. This is due to periodic transitions between the dissipation-dominated and dispersion-dominated regimes in the FAC dynamics. For conductances larger than those shown, the feedback nonlinearity has no effect on the FAC dynamics because for $\Sigma_p > 1.2$ the dissipative width is always smaller than Δx_{disp}. In this regime, the characteristic amplitude of saturation of the FLR magnetic field and the FAC scale according to $B_{sat} \sim R/\delta^{1/3}$ and $J\mu \sim R/\delta^{2/3}$, respectively.

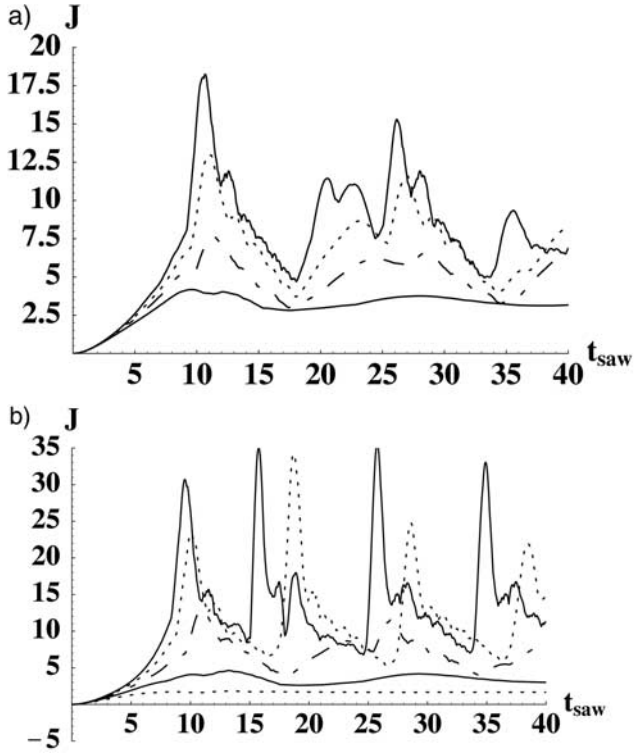

Figure 2. The field-aligned current (in $\mu A/m^2$) of the FLRs as a function of time normalized by the FLR wave period in a dipolar geometry. In the direction of increasing current strength, the five curves correspond to ambient conductance values of 0.4 mho, 0.6 mho, 0.8 mho, 1.0 mho, and 1.2 mho, respectively. The top panel corresponds to the case when the precipitation source is turned off; the bottom panel refers to the case with a precipitation source of energy 250 eV. The other parameters are the same as in Figure 1.

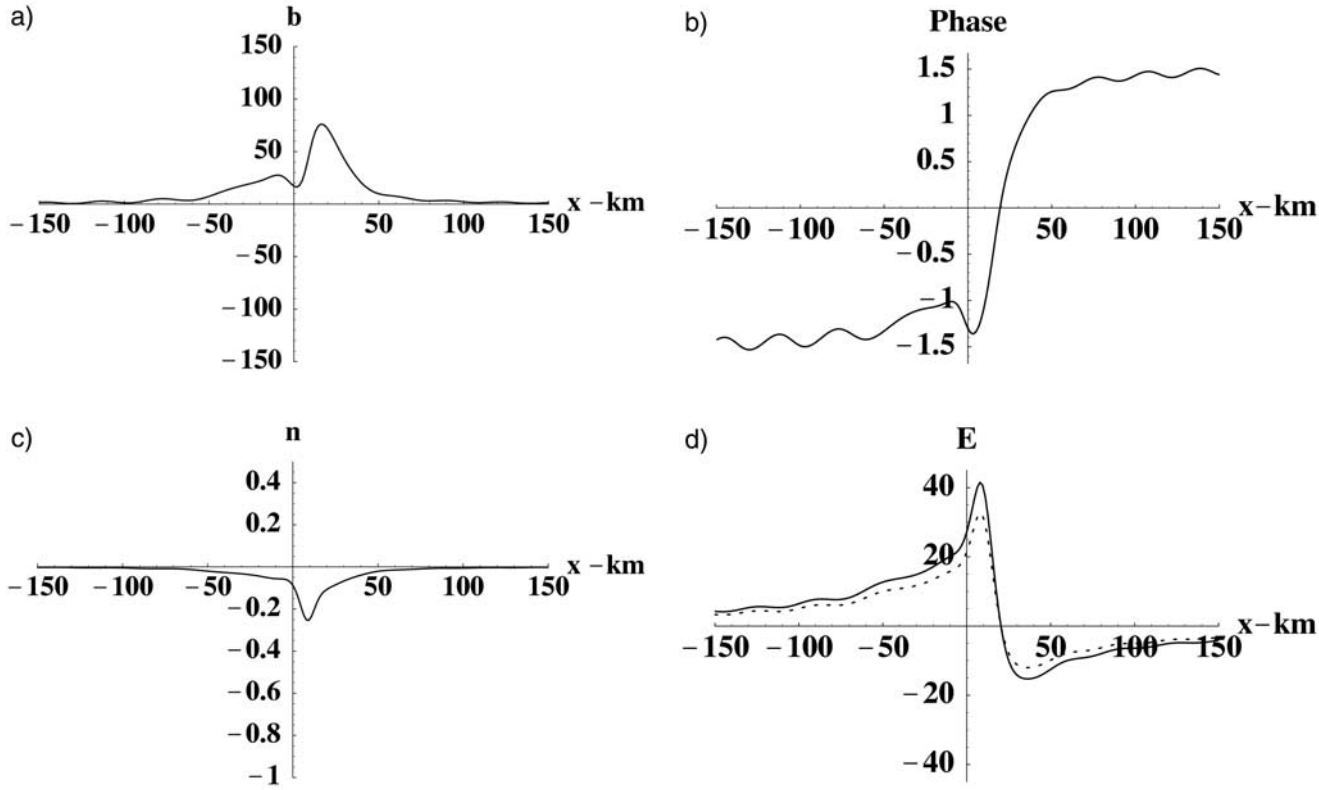

Figure 3. Radial profiles of the FLR magnetic field amplitude (in nT) and phase, the relative density perturbation (normalized by the ambient plasma density), and the in-phase (solid) and quadrature (dotted) components of the perpendicular electric field (in mV/m). Precipitation is absent, other parameters are listed in the text.

[30] Figure 2 enables us to identify the condition that should be satisfied for the feedback effect to be important:

$$\gamma_0/\omega_0 \gtrsim \left(\delta/l_\omega^2\right)^{1/3}. \tag{14}$$

This condition can be derived by comparing the dissipative width (equation 8) of the FLRs with the dispersive width (equation 7). The condition implies that initially the dissipative FLR width should be greater than the dispersive width. In this situation, the nonlinear reduction of FLR damping attempts to move the system towards the dispersive regime and a competition between these two regimes and nonlinearity results in complicated FAC dynamics and FLR structuring.

[31] Figures 3 and 4 display the radial dependence of the SAW azimuthal magnetic field, its phase, density structures, and the perpendicular electric field at a time of 10 SAW periods, corresponding to the time of occurrence of the dominant peak in Figure 1. The radial cuts are chosen at an altitude of 4000 km above the ionospheric footprint of the FLR. For a dipolar field, this corresponds to a radial scaling factor $h_x = 21.5$ when compared to the scale at the equatorial plane. The same structures would be seen at ionospheric heights with a further compression factor of 1.7. The source of electron precipitation is absent in Figure 3, while Figure 4 corresponds to a precipitation source of 350 eV electrons. Both the electric and magnetic field demonstrate a single dissipative structure for the case without precipitation where the phase changes by 180° across the resonance. In the case with precipitating electrons, the resonance structure is almost two times narrower. The narrowing and localization of the resonance is a direct consequence of the local nature of nonlinear damping. As the FLR damping decreases in the region of maximum current, it tends to enhance the current where it is already large, thus making the peak higher and narrower. This effect is even more evident in the associated density perturbations because they are driven by the ponderomotive force of SAWs, and therefore are proportional to the square of the FLR amplitude. The density structures are excited at the same position (time) where (when) the peaks of the electric and magnetic fields occur. The density cavity in Figure 4 is significantly narrower and is nearly three times deeper than the case without precipitation.

[32] The last panels in Figures 3 and 4 show the in-phase and quadrature components of the radial electric field. Both components are of the same order at the chosen altitude. Closer to the ionosphere, the in-phase component decreases and the quadrature component dominates. In contrast, at higher altitudes the quadrature component decreases and the in-phase one dominates. Later in time, SAW structures formed at the resonance propagate polewards, in the direction defined by the sign of the dispersion term in equation (1). They can be seen in Figure 5 as oscillations of the amplitude and phase of the wave magnetic field

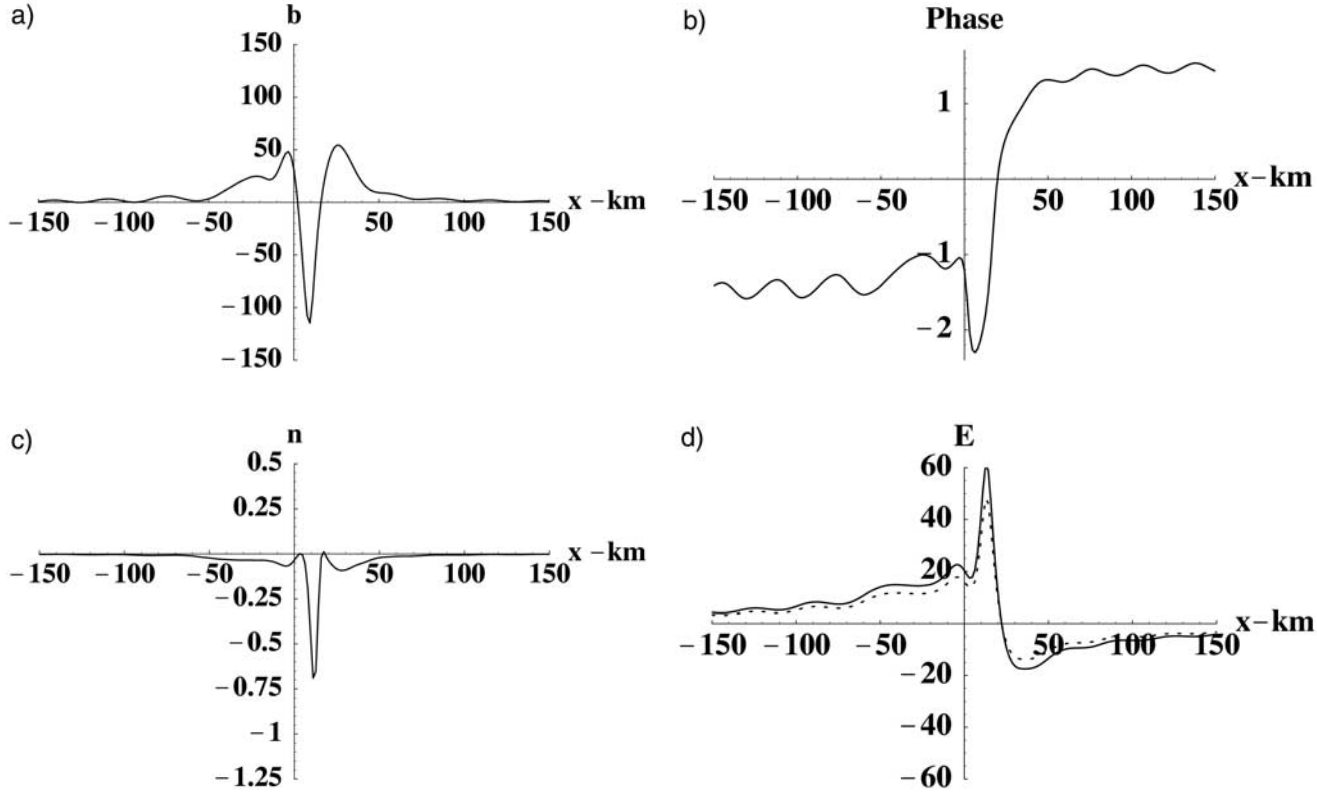

Figure 4. Radial profiles of the FLR magnetic field amplitude (in nT) and phase, the perturbed density (normalized by the ambient plasma density), and the in-phase (solid) and quadrature (dotted) components of the perpendicular electric field (in mV/m). A precipitation source of energy 350 eV is present. Other parameters are the same as in Figure 3.

along $x < 0$. These solitons are shown after 30 SAW periods, but they follow each dominant peak in Figure 1. The solitons in Figure 5 have a perpendicular width $\Delta x \sim (\delta l_\omega)^{1/3}/h_x \sim 6$ km that is defined by the balance between the dispersive and detuning terms in equation (1). Due to the surrounding low background conductance, the amplitude of the solitons reduces significantly at distances greater than 50–100 km from the position of the resonant field line. The nonlinear damping and dispersion both contribute to the slow propagation of the solitons away from the resonance, and therefore they may be viewed as a spatial structuring of the FLR associated with significant density fluctuations.

4.2. Numerical Results in a Stretched Geomagnetic Field

[33] The results presented above for a dipolar geomagnetic topology are mainly of qualitative significance. The FLR frequency of 15 mHz in that case is unrealistically high in the context of ground observations [*Samson et al.*, 1991]. Observed nightside FLRs typically fall in the range of 1–4 mHz. Since stretching of geomagnetic field lines decreases

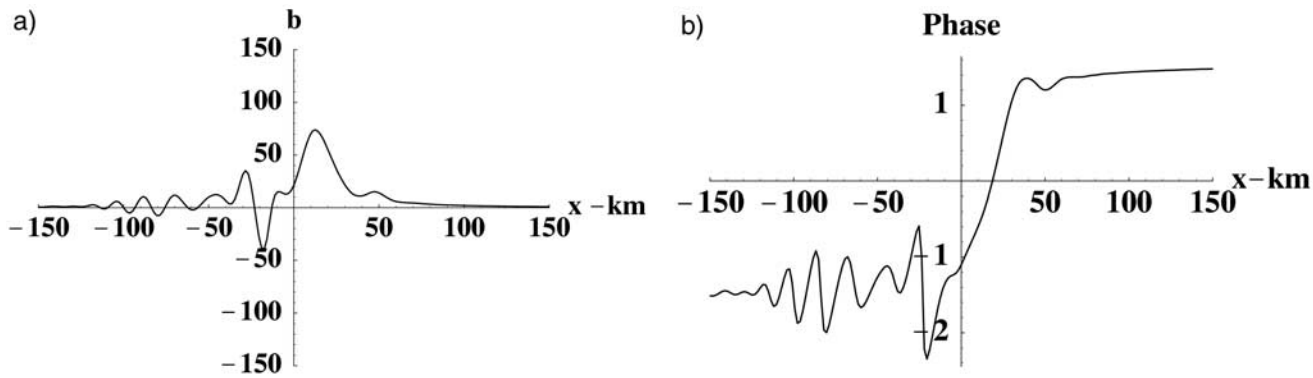

Figure 5. Radial profiles of the FLR magnetic field amplitude (in nT) and phase at the time corresponding to 30 SAW periods. The parameters are the same as in Figure 4.

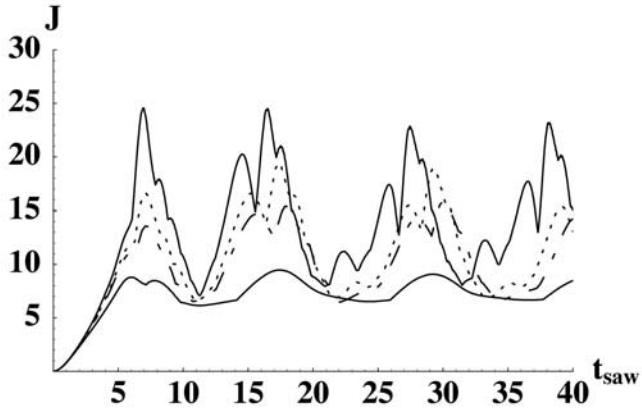

Figure 6. The field aligned current ($\mu A/m^2$) of FLRs as a function of time t normalized by the FLR wave period in a stretched geomagnetic topology (the T96 model). The solid curves correspond to the precipitation source of energy 500 eV (top curve) and to the case without precipitation (bottom curve). The dotted and dash-dotted curves correspond to the precipitation energies of 350 eV and 250 eV, respectively. The ambient conductance is 1 mho, the equatorial ion temperature is 1 keV. Other parameters are discussed in the text.

the FLR frequency [*Rankin et al.*, 2000; *Lui and Cheng*, 2001], we have extended our analysis to a stretched geomagnetic topology. The conditions chosen approximate the event reported by the FAST group [*Lotko et al.*, 1998] where the 1.3 mHz frequency of the FLR was measured by CANOPUS. We use the T96 magnetic field model described by *Tsyganenko* [1996], and refer the reader to Figure 2 of *Rankin et al.* [2000] for the topology of the field line that we use. The inputs to the T96 model are $D_{st} = -30$ nT, $B_y = 0$, $B_z = -3$ nT and dynamical solar wind pressure is 2 nPa. The field line that corresponds to $L = 6$ in a dipolar field, supports an FLR frequency $\sim$4 mHz for the same plasma parameters in the plasma sheet as in the dipolar case. It is stretched by the solar wind such that it intercepts the equatorial plane at 10.5 R_E. The frequency detuning length $l_\omega = 3\ R_E$ and the SAW damping $\gamma_0/\omega_0 = 0.076$ corresponds to the background Pedersen conductance $\Sigma_0 = 1.0$ mho. The dispersion parameter $\delta = 0.8 \cdot 10^{-3} R_E^2$ was calculated using the kinetic theory [*Tikhonchuk and Rankin*, 2000] and the driver amplitude $R = 8.1 \cdot 10^{-2}$ was chosen to fit the magnetic field amplitude with observations. In spite of larger values of the dispersion and damping that are used in the dipolar case, the parameters chosen agree with the optimum condition (equation 14) for ionospheric feedback: $\Delta x_{diss} = 0.23\ R_E$ is slightly larger than $\Delta x_{disp} = 0.13\ R_E$.

[34] In Figure 6, we present results that can be compared with Figure 1 for the case of a dipolar field. The figure shows the FAC at 4000 km altitude when the driver is continuously on. The curves correspond to cases without precipitation (bottom solid curve), and with precipitation energies of 250 eV, 350 eV, and 500 eV. Generally, because of the higher relative wave damping, the precipitation energies required to initiate the feedback effect are higher than in the case of a dipolar field. In Figure 7, we show the dependence of the FAC on the ambient conductance for cases with and without precipitation in the stretched topology. The five curves correspond to conductance values from 0.4 mho to 1.2 mho. Comparing the top (without precipitation) and bottom (precipitation energy of 350 eV) panels we note that the feedback is effective for conductance values greater than 0.8 mho where the dissipative width is nearly two times larger than the dispersive width. Comparing Figure 7 with the similar results for the dipolar geometry shown in Figure 2, one sees that at lower frequencies, feedback is stronger for the same background conductance and the period of nonlinear pulsations is longer.

[35] In Figure 8, we demonstrate the FLR dynamics for a colder plasma by reducing the equatorial ion temperature to 200 eV. At a lower plasma temperature the ion mode frequencies are smaller and the ponderomotive force excites many ion-modes which exhibit chaotic behavior. The FAC peaks are stronger and the period of nonlinear pulsations is shorter. Also, due to the continual redistribution of energy over different ion modes, the FLR is highly structured in contrast with the warmer plasma case discussed above. This

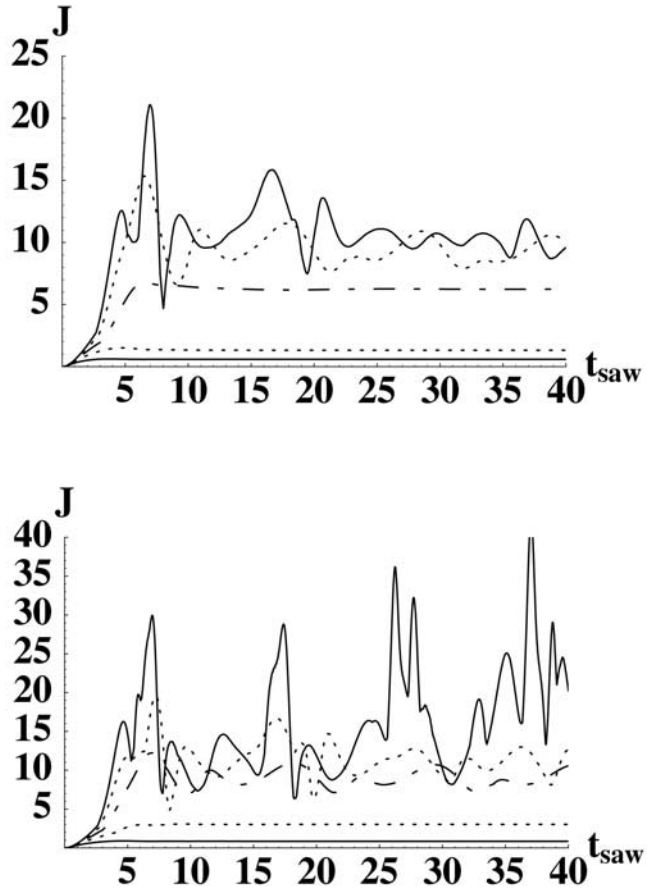

Figure 7. The field-aligned current ($\mu A/m^2$) of the FLRs as a function of time t normalized by the FLR wave period in a stretched topology. In the direction of increasing current strength, the five curves correspond to ambient conductance values of 0.4 mho, 0.6 mho, 0.8 mho, 1.0 mho, and 1.2 mho, respectively. The top panel corresponds to the case when the precipitation source is turned off; the bottom panel refers to the case with a precipitation source of energy 350 eV. The other parameters are the same as in Figure 6.

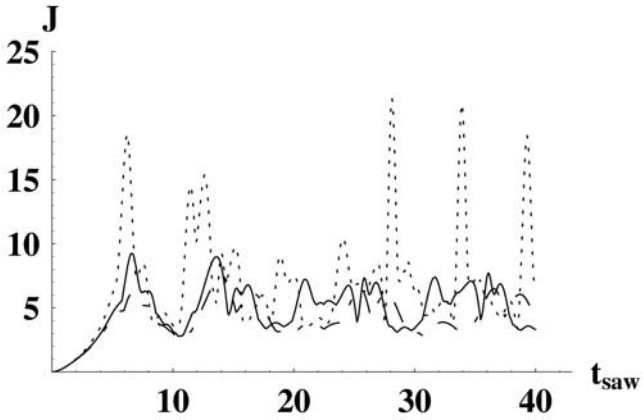

Figure 8. The field aligned current (in $\mu A/m^2$) of FLRs calculated in the stretched topology of magnetic field lines. The equatorial ion temperature is 200 eV. The curves correspond to electron precipitation energies of 1 keV (dotted curve), 500 eV (solid curve), and 350 eV (dashed curve). The ambient conductance is 1 mho, other parameters are listed in Figure 6.

is shown in Figure 9 for the cold plasma case with $T_i = 200$ eV at the equatorial plane. The electric and magnetic fields demonstrate multiple peaks of comparable amplitude with a spatial scale of the order of 10 km. Note that although the dissipative and dispersive scales in the equatorial plane are more than ten times larger than those in the dipolar case, the scales of the FLR structure at the ionospheric level are of the same order due to the much larger radial compression factor in the stretched geometry.

[36] The FLR structuring is further demonstrated in Figure 10, where we show a sequence of radial FAC profiles at 4000 km altitude during the nonlinear evolution of the FLR. Three time periods are indicated, corresponding to intervals where solitons are forming (8 periods), being emitted from the resonance (12 periods), and reforming (16 periods). It can be observed that intense currents (around 10 $\mu A/m^2$) are associated with smaller perpendicular scales of roughly 10 km (5 km above the ionosphere). They form at the resonance position and then shift polewards.

5. Summary and Conclusions

[37] We have developed a nonlinear model of FLRs to determine the temporal evolution and spatial structure of auroral arcs produced by standing SAWs on closed geomagnetic field lines. The important new elements of the model are nonlinear ionospheric feedback effects and stretched geomagnetic topology. Feedback results in an enhancement of the ponderomotive force and in a spatial structuring of 1–4 mHz FLR wave fields at modest wave amplitudes.

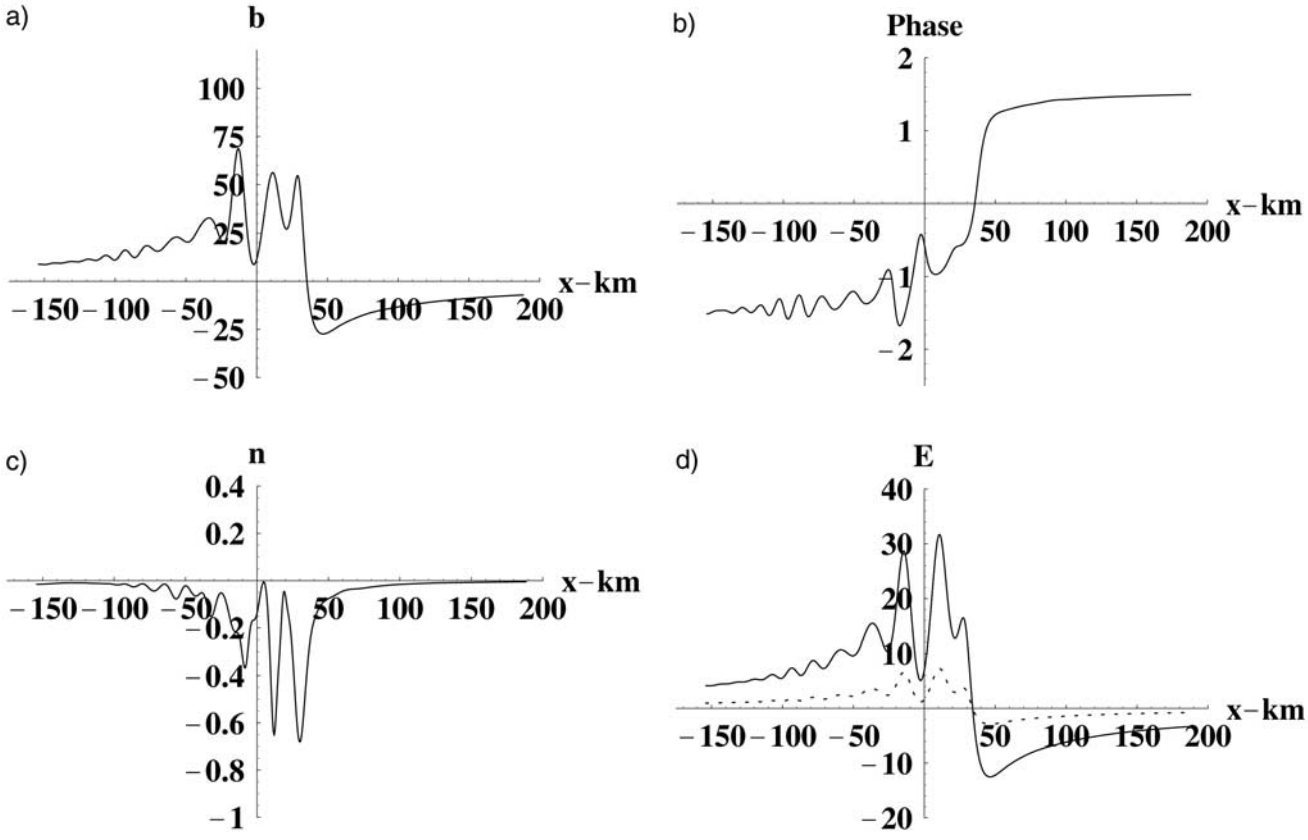

Figure 9. Radial profiles of the FLR magnetic field amplitude (in nT) and phase, the perturbed density (normalized by the ambient plasma density), and the in-phase (solid) and quadrature (dotted) components of the perpendicular electric field (in mV/m) at the time corresponding to 12 SAW periods. A precipitation source of energy 1 keV is present. Other parameters are the same as in Figure 6.

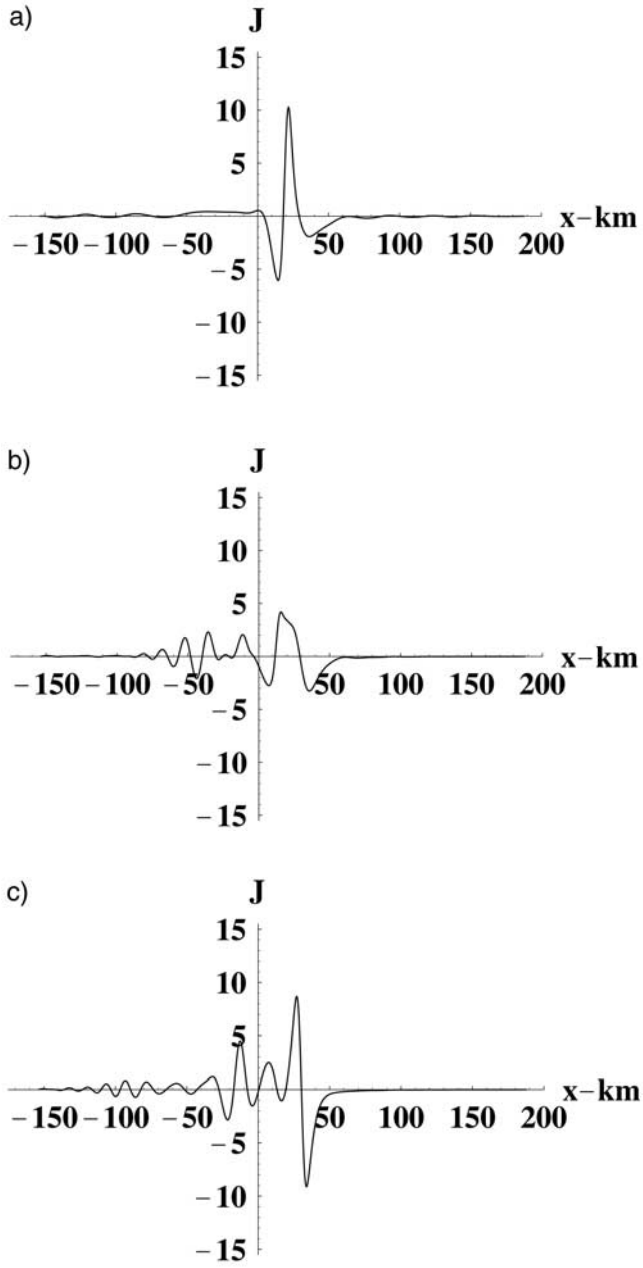

Figure 10. The radial profile of the FAC (in $\mu A/m^2$) at the altitude of 4000 km. The three panels correspond to times at 8 periods (top panel), 12 periods (middle panel), and 16 periods (bottom panel). A precipitation source of energy 1 keV is present. The other parameters are the same as in Figure 6.

[38] Our mechanism of ionospheric feedback is different from the ionospheric feedback instability discussed in the past [*Atkinson*, 1970; *Holzer and Sato*, 1973; *Lysak*, 1986, 1990, 1991; *Lyatsky and Hamza*, 2000] for the following reasons:

1. The energy to drive the ionospheric feedback instability is provided by a steady convective magnetospheric flow, while the source of FLR energy is provided by global compressional waves that resonantly mode convert to shear Alfvén waves in the inhomogeneous inner magnetosphere.

2. The feedback instability operates in the domain of roughly 0.1–1 Hz, while the feedback effect in our studies is relevant at much lower frequencies of a few mHz.

3. The feedback instability is a linear effect with respect to the SAW amplitude. It arises due to a phase difference between density and current perturbations in the ionosphere. In particular, it corresponds to a transfer of energy from the ionosphere into the magnetosphere. In contrast, the feedback effect discussed in the present work is not an instability. The FAC of the SAW is determined by Ampere's law, and evolves self-consistently. The FAC contributes to a decrease of ionospheric damping and this produces a nonlinear feedback response.

[39] We have identified the condition (equation 14) for feedback interactions to take place, and have examined the dependence of the FAC magnitude on the energy of precipitating electrons. Electrons with energies in the range of hundreds of eV can produce strong enhancements of the FAC, and correspondingly strong density depletions at auroral altitudes. The FLR structuring also increases if the background ion temperature is low, because it enhances the role played by the ponderomotive force. In this regime, precipitation, nonlinear and dispersive effects all play important roles, and relatively high precipitation energies (from 500 eV to 1 keV) are required to produce significantly enhanced FACs. However, in this strongly nonlinear regime, FLRs are significantly structured at modest wave amplitudes compared to the case without precipitation effects.

[40] Our studies in a stretched topology are qualitatively similar to those in a dipolar field. However, wave damping is stronger, and electron precipitation energies required to initiate Pedersen conductance enhancements are larger, although still in the range of hundreds of eV. We find very enhanced FACs, with magnetic energy concentrated in narrow spatial regions (roughly 5 km above the ionosphere) that can potentially explain the formation of auroral arcs in the observed frequency range of 1–4 mHz. The model results are in qualitative agreement with satellite and ground based observations of discrete auroral structures, and suggest that FAC modulation by electron precipitation is important in the dynamical nonlinear evolution of discrete auroral arcs.

[41] The nonlinear feedback effect is more pronounced at lower ionospheric conductances on the order of 1 mho. In this respect, our findings are in agreement with the statistical studies of *Newell et al.* [1996], who reported that discrete auroral arcs are more frequent in winter and at night, when the ionospheric ionization is at its minimum. Although the auroral arcs in their studies have larger mean spatial scales of 28–35 km, we believe the mechanism of arc formation is common. The ionosphere plays an active role and the background conductance is a key parameter. Future work in this direction may therefore shed more light on the nature of FLR-sustained auroral arcs, and how they relate to a wider range of auroral arc scales.

[42] **Acknowledgments.** This research was supported in part by the NSF/POWRE award ATM-9900905, by the National Science and Engineering Research Council of Canada, and the Canadian Space Agency.

[43] Arthur Richmond thanks Vincent Genot and another reviewer for their assistance in evaluating this paper.

References

Akasofu, S.-I., Thickness of an active auroral curtain, *J. Atmos. Terr. Phys.*, *21*, 287, 1961.

Atkinson, G., Auroral arc: Results of the interaction of a dynamic magnetosphere with the ionosphere, *J. Geophys. Res.*, *75*, 4746, 1970.

Borovsky, J. E., Auroral arc thickness as predicted by various theories, *J. Geophys. Res.*, *98*, 6101, 1993.

Borovsky, J. E., D. M. Suszcynsky, M. I. Buchwald, and H. V. Dehaven, Measuring the thickness of auroral curtains, *Arctic*, *44*, 231, 1991.

Frycz, P., R. Rankin, J. C. Samson, and V. T. Tikhonchuk, Field line resonances: Dispersive effects, *Phys. Plasmas*, *5*, 3565, 1998.

Génot, V., P. Louran, and F. Mottez, Electron acceleration by Alfvén waves in density cavities, *J. Geophys. Res.*, *105*, 27,611, 2000.

Goertz, C. K., Kinetic Alfvén waves on auroral field lines, *Planet. Space Sci.*, *32*, 1387, 1984.

Greenwald, R. A., and A. D. M. Walker, Energetics of long period resonant hydromagnetic waves, *Geophys. Res. Lett.*, *7*, 745, 1980.

Harel, M., R. A. Wolf, P. H. Reiff, R. W. Spiro, W. J. Burke, F. J. Rich, and M. Smiddy, Quantitative simulation of a magnetospheric substorm, 1, Model logic and review, *J. Geophys. Res.*, *86*, 2217, 1981.

Hasegawa, A., Particle acceleration by MHD surface wave and formation of aurora, *J. Geophys. Res.*, *81*, 5083, 1976.

Holzer, T. E., and T. Sato, Quiet auroral arcs and electrodynamic coupling between the ionosphere and the magnetosphere, 2, *J. Geophys. Res.*, *78*, 7330, 1973.

Hughes, W. J., Magnetospheric ULF waves: A tutorial with a historical perspective, in *Solar Wind Sources of Magnetospheric Ultra-Low Frequency Waves*, *Geophys. Monogr. Ser.*, vol. 81, edited by M. J. Engebretson, K. Takahashi, and M. Scholer, p. 1, AGU, Washington, D. C., 1994.

Kivelson, M. G., and D. J. Southwood, Coupling of global magnetospheric MHD eigenmodes to field line resonances, *J. Geophys. Res.*, *91*, 4345, 1986.

Kletzing, C., C. Cattell, F. S. Mozer, S.-I. Akasofu, and K. Makita, Evidence for electrostatic shocks as source of discrete auroral arcs, *J. Geophys. Res.*, *88*, 4105, 1983.

Knudsen, D. J., Spatial modulation of electron energy and density by nonlinear stationary inertial Alfvén waves, *J. Geophys. Res.*, *101*, 10,761, 1996.

Knudsen, D. J., E. Donovan, L. L. Cogger, B. Jackel, and W. Shaw, Width and structure of mesoscale optical arcs, *Geophys. Res. Lett.*, *28*, 3573, 2001.

Lotko, W., A. V. Streltsov, and C. W. Carlson, Discrete auroral arc, electrostatic shock and suprathermal electrons powered by dispersive anomalous resistivity, *Geophys. Res. Lett.*, *25*, 4449, 1998.

Lui, A. T. Y., and C. Z. Cheng, Resonance frequencies of stretched magnetic field lines based on a self-consistent equilibrium magnetospheric model, *J. Geophys. Res.*, *106*, 25,793, 2001.

Lyatsky, W., and A. M. Hamza, Magnetosphere-ionosphere coupling feedback instability for auroral arc generation, *Ann. Geophys.*, *18*, 1108, 2000.

Lyons, L. R., Generation of large-scale regions of auroral currents, electric potentials, and precipitation by the divergence of the convection electric field, *J. Geophys. Res.*, *85*, 17, 1980.

Lysak, R. L., Coupling of the dynamic ionosphere to auroral flux tubes, *J. Geophys. Res.*, *91*, 7047, 1986.

Lysak, R. L., Electrodynamic coupling of the magnetosphere and ionosphere, *Space Sci. Revs.*, *52*, 33, 1990.

Lysak, R. L., Feedback instability of the ionospheric resonance cavity, *J. Geophys. Res.*, *96*, 1553, 1991.

Maggs, J. E., and T. N. Davis, Measurements of the thicknesses of auroral structures, *Planet. Space Sci.*, *16*, 205, 1968.

Newell, P. T., C.-I. Meng, and S. Wing, Suppression of discrete aurorae by sunlight, *Nature*, *381*, 766, 1996.

Persoon, M., D. A. Gurnett, W. K. Petersen, J. H. Waite Jr., J. L. Burch, and J. L. Green, Electron density depletion in the nightside auroral zone, *J. Geophys. Res.*, *93*, 1871, 1988.

Prakash, M., and R. L. Lysak, Anomalous resistivity due to weak double layers, Model for Auroral Arc Thickness, *Geophys. Res. Lett.*, *19*, 2159, 1992.

Prakash, M., and R. Rankin, Role of ionospheric effects and plasma sheet dynamics in the formation of auroral arcs, *Space Sci. Revs.*, *95*(1/2), 513, 2001.

Rankin, R., P. Frycz, V. T. Tikhonchuk, and J. C. Samson, Ponderomotive saturation of magnetospheric field line resonances, *Geophys. Res. Lett.*, *22*, 1741, 1995.

Rankin, R., J. C. Samson, V. T. Tikhonchuk, and I. Voronkov, Auroral density fluctuations on dispersive field line resonances, *J. Geophys. Res.*, *104*, 4399, 1999a.

Rankin, R., J. C. Samson, and V. T. Tikhonchuk, Discrete auroral arc and nonlinear dispersive field line resonances, *Geophys. Res. Lett.*, *26*, 663, 1999b.

Rankin, R., J. C. Samson, and V. T. Tikhonchuk, Parallel electric fields in dispersive shear Alfvén waves in the dipolar magnetosphere, *Geophys. Res. Lett.*, *26*, 3601, 1999c.

Rankin, R., F. Fenrich, and V. T. Tikhonchuk, Shear Alfvén waves on stretched magnetic field lines near midnight in Earth's magnetosphere, *Geophys. Res. Lett.*, *27*, 3265, 2000.

Rees, M. H., Auroral ionization and excitation by incident energetic electrons, *Planet. Space. Sci.*, *11*, 1209, 1963.

Reiff, P. H., Models of auroral-zone conductance, Magnetospheric Currents, *Geophys. Monogr. Ser.*, vol. 28, edited by T. A. Potemra, p. 180, AGU, Washington, D.C., 1984.

Robinson, R. M., R. R. Vondrak, K. Miller, T. Dabbs, and D. Hardy, On calculating ionospheric conductances from the flux and energy of precipitating electrons, *J. Geophys. Res.*, *92*, 2565, 1987.

Samson, J. C., T. J. Hughes, F. Creutzberg, D. D. Wallis, R. A. Greenwald, and J. M. Ruohoniemi, Observations of a detached, discrete arc in association with field line resonances, *J. Geophys. Res.*, *96*, 15,683, 1991.

Samson, J. C., L. L. Cogger, and Q. Pao, Observations of field line resonances, auroral arcs and auroral vortex structures, *J. Geophys. Res.*, *101*, 17,373, 1996.

Spiro, R. W., P. H. Reiff, and L. J. Maher Jr., Precipitating electron energy flux and auroral zone conductances: An empirical model, *J. Geophys. Res.*, *87*, 8215, 1982.

Streltsov, A. V., and W. Lotko, Dispersive, nonradiative field line resonances in a dipolar magnetic field geometry, *J. Geophys. Res.*, *102*, 27,121, 1997.

Streltsov, A. V., W. Lotko, J. R. Johnson, and C. Z. Cheng, Small scale dispersive field line resonances in the hot magnetospheric plasma, *J. Geophys. Res.*, *103*, 26,559, 1998.

Taylor, J. P. H., and A. D. M. Walker, Accurate approximate formulae for toroidal standing hydromagnetic oscillations in a dipolar field, *Planet. Space. Sci.*, *32*, 1119, 1984.

Tikhonchuk, V. T., and R. Rankin, Electron kinetic effects in standing shear Alfvén waves in the dipolar magnetosphere, *Phys. Plasmas*, *7*, 2630, 2000.

Trondsen, T. S., and L. L. Cogger, A survey of small scale spatially periodic distortions of auroral forms, *J. Geophys. Res.*, *103*, 9405, 1998.

Tsyganenko, N. A., Effects of the solar wind conditions on the global magnetospheric configuration as deduced from data-based modes, in *Proc. of Third Int. Conf. on Substorms (ICS-3)*, *ESA Spec. Publ.*, *SP-389*, 181, 1996.

Xu, B. L., J. C. Samson, W. W. Liu, F. Creutzberg, and T. J. Hughes, Observations of optical aurora modulated by resonant Alfvén waves, *J. Geophys. Res.*, *98*, 11,531, 1993.

M. Prakash, Department of Physics and Astronomy, SUNY at Stony, Stony Brook, New York 11794-3800, USA. (mprakash@nuclear.physics.sunysb.edu)

R. Rankin, Department of Physics, University of Alberta, Edmonton, Alberta, Canada T6G 2E9. (rankin@phys.ualberta.ca)

V. T. Tikhonchuk, Institut de Physique Fondamentale, Université Bordeaux 1, B.P. 120, 33175 Gradignan cedex, France. (tikhon@cenbg.in2p3.fr)